The Astrophysical Journal, 601:L79–L82, 2004 January 20
© 2004. The American Astronomical Society. All rights reserved. Printed in U.S.A.

A DISK SHADOW AROUND THE YOUNG STAR ASR 41 IN NGC 1333

Klaus W. Hodapp,[1] Christina H. Walker,[2] Bo Reipurth,[3] Kenneth Wood,[2] John Bally,[4]
Barbara A. Whitney,[5] and Michael Connelley[1]
Received 2003 July 12; accepted 2003 December 1; published 2004 January 15

ABSTRACT

We present images of the young stellar object ASR 41 in the NGC 1333 star-forming region at the wavelengths of Hα and [S II] and in the *I*, *J*, *H*, and *K* bands. ASR 41 has the near-infrared morphology of an edge-on disk object but appears an order of magnitude larger than typical systems of this kind. We also present detailed models of the scattering and radiative transfer in systems consisting of a young star surrounded by a protoplanetary disk and the whole system being embedded in either an infalling envelope or a uniform molecular cloud. The best fit to the observed morphology can be achieved with a disk of ≈200 AU diameter, immersed in a low-density cloud ($\approx 2 \times 10^{-20}$ g cm^{-3}). The low cloud density is necessary to stay below the submillimeter flux upper limits and to preserve the shadow cast by the disk via single scattering. The results demonstrate that ASR 41 is probably not inherently different from typical edge-on disk objects and that its large apparent size is due to the shadow of a much smaller disk being projected into the surrounding dusty molecular material.

Subject headings: infrared: ISM — reflection nebulae — stars: formation — stars: pre–main-sequence

1. INTRODUCTION

Young low-mass stars form by accretion of material through a disk, a process accompanied by outflow activity. When most of the nascent envelope has been dispersed in the later phases of star formation, a bipolar reflection nebula can be seen in the near-infrared if the object is observed in the plane of the disk. Under this condition the star is obscured from direct view, and therefore the total near-infrared flux is dominated by the scattered light from material above and below the disk plane. Many examples of such edge-on disks have been found recently. Most of the disks in those objects have radii inferred from the optical or near-infrared morphology that are of the order of magnitude of our solar system (i.e., ≈100 AU). The prototypical HH 30 infrared source (Burrows et al. 1996) has a radius of ≈250 AU, IRAS 04302+2247 (Lucas & Roche 1998) has a measured radius of ≈200 AU in the near-infrared, while the secondary component in the HK Tauri system (Stapelfeldt et al. 1998) has ≈105 AU radius. The objects in the Taurus star-forming region (Padgett et al. 1999) range in radius from 300 to 500 AU, and the object found by Monin & Bouvier (2000) has about a 60 AU radius. In the Ophiuchus star-forming region, Brandner et al. (2000) found ≈150 AU disk radii, while Grosso et al. (2003) report a 300 AU radius and LkHα 263C (Jayawardhana et al. 2002) has ≈150 AU radius.

Increasingly sophisticated models for these objects have been developed that treat multiple scattering, absorption, and radiative transfer by dust grains. These models reproduce many of the observed features (Whitney & Hartmann 1992, 1993; Wood et al. 1998, 2001; Whitney et al. 2003; Wolf, Padgett, & Stapelfeldt 2003), constrain the density distribution around the central star, and give information about the inclination of the disk.

In the course of a near-infrared study of the star-forming region NGC 1333 in the Per OB2 complex, we found the young star ASR 41 (Aspin, Sandell, & Russel 1994) to show the morphology of an edge-on disk object with two exceptionally large scattering lobes. The edge-on disk structure of ASR 41 has been independently discovered by Elston et al. (2003) as part of their survey of giant molecular clouds. We assume NGC 1333 to be at the same distance of 316 pc that Herbig (1998) determined for the IC 348 cluster since they are both located in the same Per OB2 molecular cloud complex.

In this Letter we present optical and infrared images of ASR 41 in combination with advanced scattering and radiative transfer models, and we argue that the unusual size of this object (radius ≈3000 AU) is not indicative of the true extent of the disk but rather is a projection effect of the shadow of a much smaller disk into the surrounding dusty molecular cloud material.

2. OBSERVATIONS AND DATA REDUCTION

The NGC 1333 region was imaged with the Quick Near-Infrared Camera (Hodapp et al. 1996) at the University of Hawaii 2.2 m telescope, on the nights of 2003 January 8 and 9 (UT), with the intent of surveying this region for substellar mass objects. The night was photometric, and observations in the *J*, *H*, and *K* Mauna Kea Observatories filter set (Tokunaga, Simons, & Vacca 2002) were obtained. The frames containing ASR 41 were part of a larger mosaic. The area surrounding ASR 41 was covered by 30 individual frames in each filter; the integration times were 150 s in *J*, 100 s in *H*, and 50 s in *K*, for total integration times of 4500 s in *J*, 3000 s in *H*, and 1500 s in *K*. Photometric calibration is based on the United Kingdom Infrared Telescope standard FS111. A difficulty is posed by the bright sources and extended emission in this and all neighboring fields. The median filtering procedure to establish the sky frames leaves small residuals at the location of the bright sources and contains large-scale gradients because of the presence of extended emission. The faint outer wings of the extended flux surrounding ASR 41 are therefore subject to artifacts from poor sky subtraction.

[1] Institute for Astronomy, University of Hawaii, 640 North A'ohoku Place, Hilo, HI 96720; hodapp@ifa.hawaii.edu, connelley@ifa.hawaii.edu.
[2] School of Physics and Astronomy, University of St. Andrews, North Haugh, St. Andrews, Fife KY16 9AD, Scotland, UK; cw26@st-andrews.ac.uk, kw25@st-andrews.ac.uk.
[3] Institute for Astronomy, University of Hawaii, 2680 Woodlawn Drive, Honolulu, HI 96822; reipurth@ifa.hawaii.edu.
[4] Astrophysical and Planetary Sciences, University of Colorado, 391 UCB, Boulder, CO 80309; bally@origins.colorado.edu.
[5] Space Science Institute, 3100 Marine Street, Suite A353, Boulder, CO 80303; bwhitney@colorado.edu.

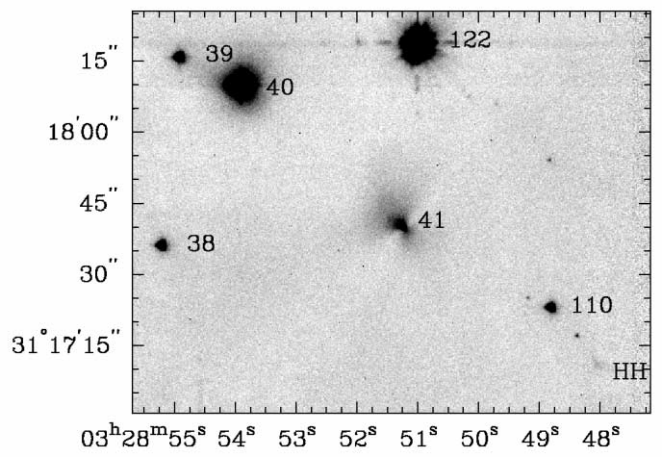

FIG. 1.—*K*-band image of ASR 41. The objects are labeled by ASR number (Aspin et al. 1994). The position of the Herbig-Haro object 727 is labeled HH.

The Hα (6569 Å/80 Å), [S II] (6730 Å/80 Å), and *I*-band (8220 Å/1930 Å) images were obtained on 2001 October 13 and 14 using the 4 m Mayall telescope at NOAO with the MOSAIC CCD camera at a scale 0.″26 pixel^{-1} (Getman et al. 2002). *I*-band photometry of ASR 41 is based on the *I*-band magnitudes of neighboring stars given by Getman et al. (2002). Images taken earlier (1997 October 29) with the same equipment were used to measure the proper motion of the newly discovered Herbig-Haro object HH 727.

3. RESULTS AND DISCUSSION

Figure 1 shows the *K*-band image of ASR 41 and its surroundings, including the Herbig-Haro object HH 727, while Figure 2 shows ASR 41 (and HH 727 as an insert) in the Hα, [S II], *I*, *J*, *H*, and *K* bands. Going from the shortest wavelength covered here (Hα) to the *J* band, the morphology of ASR 41 changes dramatically. At Hα, ASR 41 appears as a faint patch of nebulosity with a faint condensation at its center. At [S II], the central source appears brighter and the extended emission begins to show the "hourglass" shape of a bipolar nebula. The *I* band begins to show the bifurcation of the extended emission, albeit less pronounced than at the longer near-infrared wavelengths. The dark band at an angle of about 137°, bifurcating the reflection nebulosity associated with ASR 41, is most prominent from the *J* to the *K* band. The reflection nebula can be traced out to about 10″ from the center (≈3000 AU) before it gets confused with artifacts from the sky-subtraction process. The linear size of the scattering region therefore is about 10–20 times larger than in the typical edge-on disk systems listed in § 1. Either ASR 41 is a unique object surrounded by a huge extended disk or the dark band is the shadow of a much smaller (and typical) disk that is projected into the dusty material surrounding the object, as is strongly suggested by the wavelength dependence of its morphology. If the dark band were caused in its full extent by absorption in an edge-on dust disk in front of the scattering region, one would expect the dark bifurcating band to be more pronounced at shorter wavelengths. This is clearly not the case. Rather, our images suggest that the dark band is the shadow of a much smaller disk, projected into the surrounding dusty medium. The transition from single scattering at longer wavelengths, which preserves the shadow, to multiple scattering at shorter wavelengths, which fills in the shadow, occurs at wavelengths around 1 μm.

Within the dark band, a central object is clearly visible at all

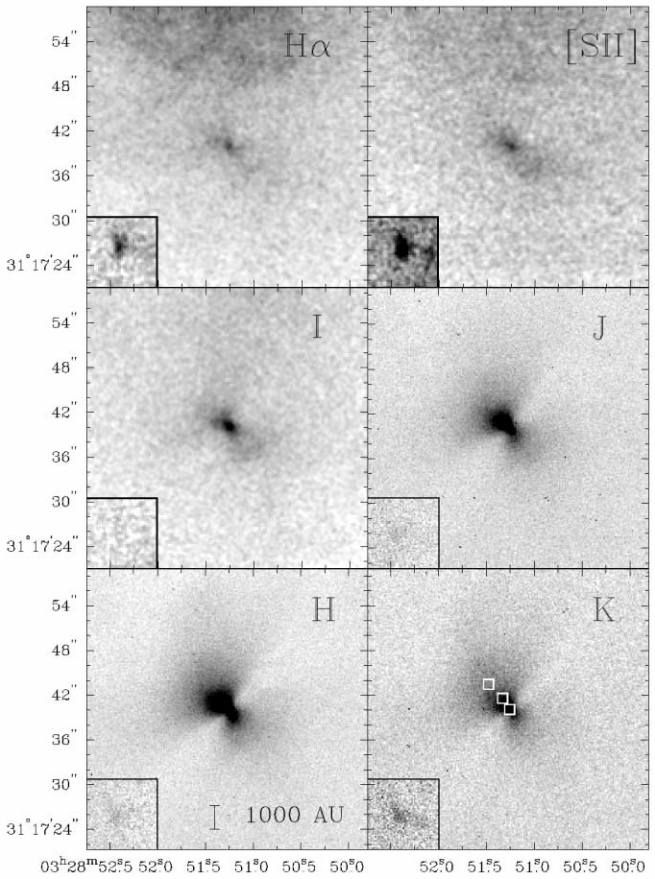

FIG. 2.—Hα, [S II], *I*-, *J*-, *H*-, and *K*-band images of ASR 41. Inserted in each image is a smaller image of the HH object 727, at the same spatial scale but with the intensity scale stretched by a factor of 2. The observed morphology of ASR 41 changes dramatically from Hα and [S II], where an extended nebula with a central almost pointlike source is visible, to the *I* band, where the bifurcating dark band becomes noticeable. The bipolar nature of the object and the full extent of the dark band are fully established in the *J* band, and the morphology then remains virtually identical in the *H* and *K* bands. The inserted image of the HH object 727 is strongest in Hα and [S II] and indicated in *K* (because of H_2 line emission) but is not detectable or very weak in the *I*, *J*, and *H* bands. Details of the morphology and photometry are discussed in § 3.

wavelengths from [S II] to the *K* band. This central object has a FWHM of 0.″69 in the *K* band, while the average FWHM of five other stars in Figure 1 is 0.″61 ± 0.″01. The central object is thus marginally different from a star; reflection nebulosity is contributing to its FWHM. Its position was measured in the *J* band relative to four stars in the USNO-B catalog (Monet et al. 2003) to be R.A. = 3^{h}28^{m}51.^{s}3, decl. = +31°17′40″ (J2000.0), with estimated errors of ≈0.″25 for the absolute coordinates. Astrometry of the central object in the [S II] image, using a larger set of USNO-B catalog stars than in the case of the infrared image, showed that it has the same coordinates as the corresponding object in the *J*-band image within the relative errors of ≈±0.″14. We do not see evidence for a wavelength-dependent position of the central brightness peak, as is often found in cometary or bipolar nebulae associated with Class I objects that are dominated by absorption from a large and massive disk (e.g., Hodapp et al. 1988).

The central source has magnitudes in a 1.″5 × 1.″5 box centered on the central object of $I = 20.2$, $J = 17.4$, $H = 16.1$, and $K = 15.3$. The central source has a color of $H-K = 0.73$ and $J-H = 1.36$, while the color of the reflection nebulosity is

bluer: We have taken measurements in 1.″5 × 1.″5 boxes at two additional positions to the northeast of the central star, i.e., in the reflection nebula, as indicated in Figure 2. In the additional box closer to the central object, we measured $H-K = 0.24$ and $J-H = 1.05$; in the box farther to the northeast we measure $H-K = 0.34$ and $J-H = 1.15$, with estimated errors in these colors of $\approx \pm 0.05$ mag. This is consistent with the flux from the central star and possibly the innermost parts of the reflection nebula being reddened by absorption in the small disk, and the flux in the extended reflection nebula being bluer, possibly because of preferential scattering by small dust particles.

ASR 41 is not associated with a strong submillimeter source. The object lies just at the southern tip of a ridge of extended 850 μm emission associated with the HH 12 complex (Sandell & Knee 2001), but it is not detectable as an individual point source in their map. From the fact that even the lowest contour (75 mJy beam^{-1}) of their map is not significantly distorted at the position of ASR 41, we estimate an upper limit to its 850 μm flux of 200 mJy. This implies that the total mass of dust involved in the scattering of light from the central source, and the mass of the disk around the central star, must be relatively small. This point is discussed in more detail in § 4.

To the southwest of ASR 41, a faint extended object at R.A. = $3^h28^m48^s.1$, decl. = +31°17′10″ (J2000.0) is most prominent in Hα and [S II] and faintly visible in *K* (Fig. 2, inserts). This is the photometric signature of a low-excitation Herbig-Haro object without significant [Fe II] emission in the *H* band (Reipurth & Bally 2001). The object has therefore been named HH 727. Proper-motion measurements on the [S II] images from 1997 and 2001 show a small (about 1 pixel) shift of the photocenter of the HH knot toward the southwest (P.A. = 215 ± 15). The shift corresponds to ≈100 km s^{-1} in the general direction away from ASR 41, roughly perpendicular to the plane of the bifurcating disk. While more precise measurements are clearly desirable, this strongly suggests that the HH object is physically associated with ASR 41.

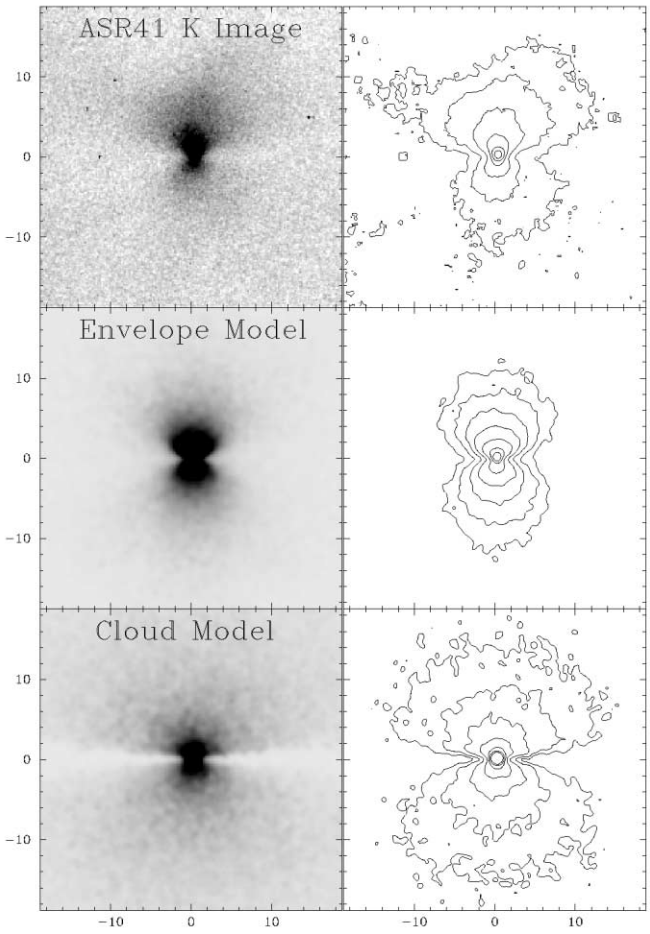

FIG. 3.—Comparison of the *K*-band image (rotated) of ASR 41 (*top panels*) with a disk+envelope model (*middle panels*) and a disk+cloud model (*bottom panels*).

4. MODELING OF THE ASR 41 DISK SHADOW

We have computed detailed models for ASR 41 using a Monte Carlo scattered light code (Whitney & Hartmann 1992, 1993) updated in Whitney et al. (2003). The models contain a number of simplifying assumptions, in particular about the grain properties, and therefore cannot be expected to reproduce all features of the observations. The main purpose of the modeling is to demonstrate that the object can be explained well within the current paradigm of star formation. The models discussed here are based on the assumption that ASR 41 is essentially a Class II T Tauri star surrounded by a disk of roughly the size of our solar system ($r \approx 100$ AU), i.e., very similar to other edge-on disk systems.

The two models differ in the assumptions about the distribution of the scattering dust surrounding the central star and its protoplanetary disk. Two types of models were considered: disk plus constant density cloud (the "disk+cloud model") and disk plus infalling envelope (the "disk+envelope model"). Both reproduce the dark band as the shadow of a smaller disk.

The geometry usually used to model young bipolar nebulae is an infalling envelope model, with the infall rate adjusted to model objects in different evolutionary classes (Whitney & Hartmann 1993; Whitney et al. 2003). For ASR 41, the infall rate is constrained by the upper limit for the submillimeter flux. The disk+envelope model in Figure 3 uses an outer disk radius of 200 AU, a disk mass of 0.06 $M_\odot$, an outer envelope radius of 7000 AU, and an infall rate of 3.5×10^{-6} $M_\odot$ yr^{-1} that is similar to the rate used in other successful models of young stellar objects (Whitney & Hartmann 1993). The infalling envelope has the density distribution of the free-fall models of Ulrich (1976) and Cassen & Moosman (1981). This model reproduces the basic features of the observations but shows a steeper intensity gradient with distance from the illuminating object than was observed. It predicts an 850 μm flux of 71 mJy, consistent with the submillimeter upper limit.

The other model is based on the assumption outlined in qualitative form earlier, that ASR 41 consists of a typical small edge-on disk object and a surrounding scattering cloud of uniform density into which the disk shadow gets projected. For this model, the density of the surrounding scattering material was adjusted so that single scattering dominates, which preserves the shadow effect and also coincidentally keeps the submillimeter flux within the observed upper limit. The "cloud model" uses a disk radius of 100 AU and a mass of 0.005 $M_\odot$; for the best fit to the *K*-band data, the cloud itself is assumed to have a radius of 10,000 AU. Our disk+cloud model assumes a cloud density of 2×10^{-20} g cm^{-3}, which is within the range of typical densities in large molecular clouds. This model produces an 850 μm flux of 40 mJy, well below the submillimeter flux limit. Increasing both the cloud density and the disk mass by an order of magnitude leads to slightly better fits to the near-infrared fluxes but predicts an 850 μm flux of 234 mJy, i.e., above the flux limit.

Figure 3 shows the *K*-band image of ASR 41 (*top*, rotated to have the polar axis vertical for comparison with the models) and the two model flux distributions. Some noise was added to the model images to make them more visually comparable to the real image. The disk+envelope model is successful at matching the photometry, but morphologically, the flux is falling off too rapidly with distance from the central source because of the density distribution in the envelope. The disk+cloud model matches the near-infrared morphology better, including the large extent of the reflection nebulosity.

Both model fits to the observed photometry indicate inclinations of about 80°, even though the match to the observed morphology, in particular the difference in flux from the two lobes, could probably be improved by assuming somewhat lower inclinations. These problems that our models have with precisely matching the near-infrared photometry and morphology of the object point to shortcomings in the dust model used here. Our code is currently limited to one dust model throughout, and given the extent of the object an interstellar grain model was chosen. This is a good approximation for the particles expected in a thin molecular cloud but may not be a good model for the grains in a much denser protoplanetary dust disk in the close vicinity of a young star (e.g., Beckwith et al. 1990; Wood et al. 2002). Because of the obvious simplifications in our model, they are not suitable to derive the luminosity or detailed information about the evolutionary state of the star at the center of ASR 41.

5. SUMMARY

We have presented images of the young stellar object ASR 41 in NGC 1333 at wavelengths ranging from Hα to the *K* band. The bipolar nebula seen at the longer of these wavelengths is much larger than typical edge-on disk systems but can be understood as the shadow of a smaller disk being projected into the dusty material of the surrounding molecular cloud. Detailed model calculations of the scattering and radiative transfer in this object have been presented. These models show that the morphological features and the near-infrared fluxes can be modeled by a small low-mass disk and surrounding scattering medium without violating the upper limit on the submillimeter flux. ASR 41 is, most likely, a Class II T Tauri star with a disk of roughly the size of our solar system and overall similar to other edge-on disk objects. It is distinguished from those objects by the scattering of the disk shadow in the surrounding dusty molecular material.

NOAO is operated by the Association of Universities for Research in Astronomy, Inc., under cooperative agreement with the National Science Foundation.

REFERENCES

Aspin, C., Sandell, G., & Russel, A. P. G. 1994, A&AS, 106, 165
Beckwith, S. V. W., Sargent, A. I., Chini, R. S., & Guesten, R. 1990, AJ, 99, 924
Brandner, W., et al. 2000, A&A, 364, L13
Burrows, C. J., et al. 1996, ApJ, 473, 437
Cassen, P., & Moosman, A. 1981, Icarus, 48, 353
Elston, R. J., et al. 2003, BAAS, 202, 28.09
Getman, K. V., Feigelson, E. D., Townsley, L., Bally, J., Lada, C. J., & Reipurth, B. 2002, ApJ, 575, 354
Grosso, N., Alves, J., Wood, K., Neuhäuser, R., Montmerle, T., & Bjorkman, J. E. 2003, ApJ, 586, 296
Herbig, G. H. 1998, ApJ, 497, 736
Hodapp, K.-W., Capps, R. W., Strom, S. E., Salas, L., & Grasdalen, G. L. 1988, ApJ, 335, 814
Hodapp, K.-W., et al. 1996, NewA, 1, 177
Jayawardhana, R., Luhman, K. L., D'Alessio, P., & Stauffer, J. R. 2002, ApJ, 571, L51
Lucas, P. W., & Roche, P. E. 1998, MNRAS, 299, 723
Monet, D. G., et al. 2003, AJ, 125, 984
Monin, L.-L., & Bouvier, J. 2000, A&A, 356, L75
Padgett, D. L., Brandner, W., Stapelfeldt, K. R., Strom, S. E., Tereby, S., & Koerner, D. 1999, AJ, 117, 1490
Reipurth, B., & Bally, J. 2001, ARA&A, 39, 403
Sandell, G., & Knee, L. B. G. 2001, ApJ, 546, L49
Stapelfeldt, K. R., Krist, J. E., Menard, F., Bouvier, J., Padgett, D. L., & Burrows, Ch. J. 1998, ApJ, 502, L65
Tokunaga, A. T., Simons, D. A., & Vacca, W. D. 2002, PASP, 114, 180
Ulrich, R. K. 1976, ApJ, 210, 377
Whitney, B. A., & Hartmann, L. 1992, ApJ, 395, 529
———. 1993, ApJ, 402, 605
Whitney, B. A., Wood, K., Bjorkman, J. E., & Wolff, M. J. 2003, ApJ, 591, 1049
Wolf, S., Padgett, D. L., & Stapelfeldt, K. R. 2003, ApJ, 588, 373
Wood, K., Kenyon, S. J., Whitney, B. A., & Turnbull, M. 1998, ApJ, 497, 404
Wood, K., Smith, D., Whitney, B., Stassun, K., Kenyon, S. J., Wolff, M. J., & Bjorkman, K. S. 2001, ApJ, 561, 299
Wood, K., Wolff, M. J., Bjorkman, J. E., & Whitney, B. A. 2002, ApJ, 564, 887